

Supplementary Information

Protein corona as the key factor governing the in vivo fate of magnetic nanoparticles

Ashish Avasthi^{a,b}, Yilian Fernandez-Afonso^c, Lucía Gutiérrez^{c,d}, Jesús M. De la Fuente^{c,d},
Manuel Pernía Leal^c, Carlos Caro^{a,b,*}, Maria Luisa Garcia Martin^{a,b,d,*}

^aBiomedical Magnetic Resonance Laboratory-BMRL, Andalusian Public Foundation Progress and Health-FPS, Seville, Spain

^bBiomedical Research Institute of Malaga and Nanomedicine Platform (IBIMA-BIONAND Platform), University of Malaga, C/Severo Ochoa, 35, 29590 Malaga, Spain

^cInstituto de Nanociencia y Materiales de Aragón (INMA), CSIC-Universidad de Zaragoza, 50009 Zaragoza, Spain

^dNetworking Research Center on Bioengineering, Biomaterials and Nanomedicine, CIBER-BBN

^eDepartamento de Química Orgánica y Farmacéutica, Facultad de Farmacia, Universidad de Sevilla, C/ Profesor García González 2, 41012 Seville, Spain

Index

1. Methods

- a) Synthesis of Iron oleate
- b) Synthesis of GA-PEG3000-OH ligand
- c) Ligand exchange
- d) Characterization
- e) Cell Culture Evaluation
- f) Animal Housing and Care
- g) *In vivo* Magnetic Resonance Imaging (MRI)
- h) AC Susceptibility Measurements
- i) Blood Collection Process
- j) Histology

2. Results

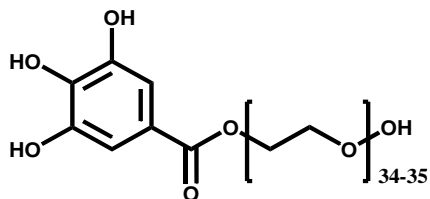
- a) Characterization
- b) Protein corona analysis
- c) Cell toxicity assessment
- d) *In vivo* MRI studies
- e) AC susceptibility measurements
- f) Histology

1. METHODS

a) Synthesis of iron oleate

Following a slightly modified previous protocol from Park et al., 10.8 g of iron chloride was mixed with 36.5 g of sodium oleate in a solution containing hexane (160 ml), ethanol (80 ml), and distilled water (60 ml). The mixture was stirred under inert conditions and temperature was increased to reflux temperature (70 °C). The reaction was allowed to continue for 4 hours before being allowed to naturally cool down. It was then washed in a separation funnel with distilled water 3 times to obtain a slurry. The slurry was then subjected to rotavapor to remove any additional solvents and attain a viscous reddish-brown slurry.

b) Synthesis of GA-PEG3000-OH ligand



The ligand was synthesized using a previously described protocol from our group.¹ To a solution of polyethylene glycol (Mw: 3000 g/mol, 1 mmol, 3.0 g), gallic acid (Mw: 170 g/mol, 1 mmol, 170 mg) and 4-(dimethylamino) pyridine (Mw: 122 g/mol, 200 μ mol, 24 mg) in 100 mL of tetrahydrofuran and 10 mL of dichloromethane, in a round bottom flask under nitrogen atmosphere, a solution of dicyclohexyl carbodiimide (Mw: 206 g/mol, 5 mmol, 1 g) in tetrahydrofuran was added dropwise. The mixture was stirred overnight at room temperature. The reaction mixture was filtered through a filter paper, and the solvents were rota-evaporated. It was filtered and dried in a lyophilizer prior to use.

c) Ligand exchange

Briefly, 50 μ l of triethylamine was added to a glass vial containing a 1.0 ml solution of NPs (10 g/l of Fe) and 1.0 ml of 0.1 M GA-PEG3000-OH solved in CHCl_3 . The mixture was sonicated for 1 h and heated to 50 °C for 4 h. It was then diluted with 5 ml of toluene, 5 ml of milli-Q water. This mixture was shaken, and the nanoparticles were transferred into the aqueous phase. The aqueous phase was collected in a round-bottom flask, and the residual organic solvents were rota-evaporated. The gallol-derived NPs were then purified in centrifuge filters with a molecular weight cut-off of 100 kDa at 450 rcf. In each centrifugation, the functionalized NPs were re-suspended with milli-Q water. The purification step was repeated several times until the filtered solution was clear. After purification, the gallol-derived NPs were resuspended in PBS buffer. Finally, to ensure

highly stable mono-dispersed NPs, this solution was centrifuged at 150 rcf for 5 min and placed onto a permanent magnet (0.6 T) for 5 min.

d) Characterization of IONPs

Transmission Electron Microscopy (TEM). TEM samples were prepared by dropping a solution of the PEGylated magnetic nanoparticles (approximately 1 g/L of Fe) on a carbon-coated copper grid and further drying at room temperature. TEM images were obtained on a FEI Tecnai G2 Twin microscope operated at an accelerating voltage of 100 kV. The mean diameter was calculated for each nanoparticle by measuring around a hundred nanoparticles.

X-ray diffraction (XRD). The nanoparticles suspension was dried in a thermoblock at 50 °C until ~ 1 mg of dry powder was obtained, which was then used for further analysis. Laboratory X-ray powder diffraction (XRPD) patterns were collected on a PANalytical EMPYREAN automated diffractometer. Powder patterns were recorded in Bragg-Brentano reflection configuration by using the PIXcel 3D detector with a step size of 0.017° (2 θ). The powder patterns were recorded between 4 and 70 in 2 θ with a total measuring time of 30 min. The patterns were analyzed by the High Score Plus (PANalytical software) employing the PDF4 database.

Inductively Coupled Plasma High-Resolution Mass Spectroscopy (ICP-HRMS). Briefly, 2.5 mL of aqua regia were added to 25 μ L of a solution of nanoparticles in a volumetric flask. The mixture was left overnight. Then, milli-Q water was added to complete the total volume of 25 mL. Quantitative analysis was performed using an inductively coupled plasma mass spectrometer (ICP-MS), NexION 300D (PerkinElmer), equipped with a single quadrupole analyzer and a collision cell using helium gas. ICP-MS analysis is based on a physical method that detects ions in their M⁺ state. An inductively coupled plasma system is used to generate these ions. The resulting ion spectrum is measured using a quadrupole mass spectrometer. This is achieved through an interface zone that introduces the ions from the plasma via a triple-cone system, employing a differential vacuum unit, and focuses the ions toward the collision/reaction cell through a quadrupole ion deflector. For quantitative analysis, a calibration curve was generated using external calibration based on nine points: one blank and eight calibration standards prepared from a 10 ppm multielemental solution, along with the inline addition of an internal standard.

Instrumental conditions during analysis were as follows:

- Nebulizer gas flow: 0.92 L/min
- Plasma gas flow: 18 L/min
- Auxiliary gas flow: 1.2 L/min
- Helium flow (collision mode): 3 mL/min
- RF power (ICP): 1600 W

Concentration calculations were performed using Syngistix 2.5 software (PerkinElmer), incorporating relevant dilution data.

Fourier Transform Infra-Red Spectroscopy (FTIR). The nanoparticles suspension was dried in a thermoblock at 50 °C until ~ 1 mg of dry powder was obtained, which was then used for further analysis. FTIR spectra were obtained in an FTIR-4100 Jasco equipped with an ATR accessory (MIRacle ATR, PIKE Technologies) coupled to a liquid nitrogen-cooled mercury cadmium telluride (MCT) detector. Resolution was set at 2 cm⁻¹, accumulating 50 scans in the 4000 to 500 cm⁻¹ range.

¹H Nuclear magnetic resonance spectroscopy (NMR). ¹H-NMR spectra were acquired on a Bruker Ascend 400 MHz NMR spectrometer.

Thermogravimetric analysis (TGA). The nanoparticles suspension was dried in a thermoblock at 50 °C until ~ 1 mg of dry powder was obtained, which was then used for further analysis using a METTLER TOLEDO model TGA/DSC 1 in the temperature range of 30–800 °C with a heating rate of 10 °C/min under a N₂ flow (50 mL/min).

Dynamic Light Scattering (DLS). The size distribution and zeta potential measurements of the PEGylated NPs were performed on a Zetasizer Nano ZS90 (Malvern, USA). The NPs were dispersed in PBS at a concentration of 100 mg/L of Fe. The measurements were done on a cell type: ZEN0118-low volume disposable sizing cuvette, setting 2.420 as refractive index and with 90° as angle of detection. The measurement duration was set as automatic, and three as the number of measurements.

PEG conformation and Packing density calculation. This conformation is dependent on the Flory radii of PEG₃₀₀₀. This radius is defined as:

$$R_F = \alpha N^{3/5}$$

Where R_F is the Flory radii, α is the length of the ethoxy unit (0.35nm), and N is the extent of polymerization. This radius, when calculated for PEG₃₀₀₀, turns out to be ~ 4.3 nm, while the distance between points where PEG was grafted could be calculated as:

$$D = 2 \sqrt{\frac{A}{\pi}}$$

where D is the distance, and A is the area occupied by the PEG chain. This area could be further calculated as:

$$A = \frac{1}{\sigma} = \frac{S}{N}$$

where σ is the coverage density of PEG and S is the total surface area of NPs.

The distance between two consecutive gallol-PEG ligands was thereafter calculated for both 4 nm and 8 nm particles. It turned out to be 0.78 and 1.58 nm, respectively. So, for 4 nm particles, D < R_F, and for 8 nm particles also D < R_F, which illustrates the stretch of polymer to be dense brush-like.²

³ Normally, one would imagine the PEG chain to be linear on the surface, but as the density increases on the surface, PEG exerts osmotic pressure in the media, causing the PEG chains to curl up and form brush conformation. When this surface density increases further, it forms dense brush-like conformation, as is the case for our IONPs. The length of the grafted layer can be calculated by:

$$L = \frac{N\alpha^{\frac{5}{3}}}{D^{\frac{2}{3}}}$$

which gives the length or thickness of GA-PEG3000-OH ligand bound to 4 nm and 8 nm particles to be around 13.32 nm and 8.32 nm respectively. This thickness explains the similar HDD obtained by 4 nm and 8 nm particles. It is important to note that despite having the same ligand, the thickness of PEG bound to the particles is different. This is due to the different core sizes of the particles and the way PEG orients itself on the surface, along with its packing density.

The packing density was calculated using the formula:

$$\rho = \frac{\text{Total number of molecules of ligand}}{S_{\text{Total NP}} (\text{nm}^2)}$$

where $S_{\text{Total NP}}$ is Total surface area. Molecular weight for GA-PEG3000-OH was taken to be 3152 g/mol, and the density of magnetite was taken as 5.17.

Superconducting Quantum Interference Device (SQUID) Magnetometry measurements. To characterize the NPs, a known volume of the colloid was deposited on a piece of cotton wool and allowed to dry. Then, the sample was placed inside a gelatin capsule. For the tissue characterization, organs were freeze-dried and placed directly in the gelatin capsule, except for the liver, which was ground to powder to generate a homogeneous sample, and then a part was weighted and placed inside the gelatin capsule. The temperature dependence of the AC magnetic susceptibility was measured using a Quantum Design (USA) MPMS-XL SQUID magnetometer in the range of 2-200 K, with a frequency of 11 Hz and magnetic field strength of 326 A/m.

In vitro transverse relaxivities (r_2). ¹H NMR transverse relaxation times, T_2 , were measured at 1.5 T (Bruker Minispec) using the Carl–Purcell–Meiboom–Gill (CPMG) sequence, with concentrations of nanoparticles ranging between 2 and 0.125 mM of Fe at 37° C. r_2 was calculated from the slope of the linear fit of the relaxation rate ($1/T_2$) versus NPs concentration as indicated in the following equation:

$$\frac{1}{T_2} = \frac{1}{T_2(0)} + r_2[\text{Fe}]$$

Proteomics. In order to perform the protein corona analysis, 100 μL (approximately 1 mg/mL) of both NPs were diluted in 900 μL of FBS and incubated for 1 h at room temperature ($n = 2$, conducted on different days to increase the biological replicates across various days). Then, NPs

were centrifuged at 10000 r.p.m. for 20 min and washed 3 times with PBS. Proteins were eluted from NPs by gel-assisted proteolysis, as previously described.⁴ Gel-assisted proteolysis: 45 μ L of sample was mixed with 14 μ L of 40% acrylamide monomer solution and 2.5 μ L of 10% ammonium persulfate. At this point, 1 μ L of TEMED was quickly added. The mixture was allowed to fully polymerize for 20 min before gel digestion. Gels were cut into 1-2 mm cubes and treated with 50% acetonitrile (ACN)/25 mM ammonium bicarbonate using a scalpel. Then, samples were dehydrated and dried with CAN before being reduced with 10 mM DTT in 50 mM ammonium bicarbonate for 30 min at 56 °C. Subsequently, excess DTT was removed, and the cysteine residues were carbamidomethylated with 55 mM iodoacetamide in 50 mM ammonium bicarbonate for 20 min at room temperature (in dark conditions). After the carbamidomethylation, the gel pieces were dehydrated again. Later, the proteins were digested by rehydrating the gel pieces in 10 ng/ μ L trypsin solution (Promega) and incubating at 30 °C overnight. Peptides were extracted from the gel pieces with ACN/0.1% formic acid (FA) for 30 min at room temperature. Samples were dried in a SpeedVac™ vacuum concentrator to remove residual ACN and ammonium bicarbonate, redissolved in 0.1% FA, and sonicated for 3 min, followed by centrifugation at 13000 g for 5 min. Finally, the samples were purified and concentrated using C18 ZipTip® (Merck).

The HPLC mobile phases were:

-solvent A: 0.1% FA in water

-solvent B: 0.1% FA in 80% ACN.

From a thermostatted autosampler, 1 μ L (100 ng) was automatically loaded into a trap column (Acclaim PepMap 100, 75 μ m \times 2 cm, C18, 3 μ m, 100 Å, Thermo Fisher) at a flow rate of 20 μ L/min and eluted down in a 50 cm analytical column (PepMap RSLC C18, 2 μ m, 100 Å, 75 μ m \times 50 cm, Thermo Fisher). Peptides were eluted from the analytical column with a 60 min gradient from 5% to 20% solvent B, followed by a 5 min gradient from 20% to 32% solvent B, and finally to a 95% Solvent B for 10 min before re-equilibrating with 5% Solvent B at a constant flow rate of 300 nL/min. Then, samples were measured in a quadrupole-linear trap-Orbitrap Q-Exactive HF-X mass spectrometer (ThermoFisher Scientific). Data were acquired using Tune 2.9 and Xcalibur 4.1.31.9 (Thermo Fisher), performed in electrospray ionization positive mode. MS1 scans were acquired from m/z 300–1750 at a resolution of 120000. With a data-dependent acquisition method, the 20 most intense precursor ions with + 2 to + 5 charges were isolated within a 1.2 m/z window and fragmented to obtain the corresponding MS/MS spectra. The fragment ions were generated in a higher-energy collisional dissociation cell with a fixed first mass at 110 m/z and detected by the Orbitrap mass analyzer at a resolution of 30000. Raw data were analyzed with Proteome Discoverer 2.4 software (Thermo Fisher Scientific). The MS2 spectra were identified by using the search engine Sequest HT (mass tolerance of 10 ppm and 0.02 Da), and the Swiss-Prot part of UniProt for *Mus musculus* was utilized as the database. Protein assignments were validated using the Percolator algorithm by imposing a strict 1% false discovery rate (FDR) cutoff. Label-free quantitation was implemented using the Minora feature of Proteome Discoverer™ 2.4. Protein

abundance ratios were directly calculated from the grouped protein abundances. ANOVA was based on the abundance of individual proteins or peptides.

PepStat analysis of the obtained protein corona. Isoelectric point, the number of residues, and the amino acid composition of both unique and common proteins of the protein corona were analyzed using the EMBOSS suite program PepStat.

e) Cell Culture Evaluation

Cell Culture. HFF-1 human foreskin fibroblast cells were cultured in Dulbecco's Modified Eagle Medium (DMEM). Medium was supplemented with 2 mM L-glutamine, 10% fetal bovine serum (FBS) and 1% penicillin/streptomycin. Cells were incubated at 37 °C with a humidified atmosphere containing 5% CO₂.

Cell morphology studies and “live-dead” assay. The HFF-1 cells were plated at a density of 1x10⁴ cells/well in a 96-well plate at 37 °C in 5% CO₂ atmosphere (100 µl per well, number of repetitions = 5). After 24 h of culture, the medium in the wells was replaced by fresh media containing the NPs in varying concentrations from 0.1 to 100 µg (Fe) /mL. After 24 h, Triton X-100 was added to the positive control wells. All the wells were stained after 15 min with: 1) DAPI (4',6-diamidino-2-phenylindole, dilution 1:3000 in PBS) to label cells nuclei, although with stronger labeling in live cells; 2) calcein (1:1000 in PBS) to evaluate cell activity and 3) TO-PRO-3 iodine to label dead cells (dilution 1:1000 in PBS). Cell morphology images were acquired with a Perkin Elmer Operetta High Content Imaging System with a 20×LWD 0.45 NA air objective lens. Five well replicates for each condition were analyzed, with 10 random image fields captured per well. For each field, fluorescence images for DAPI, Calcein-AM, and TO-PRO-3, plus a brightfield image, were captured. Cell mortality percentages were calculated automatically by Operetta Harmony software, whereby all nuclei (dead and alive) were identified from the DAPI staining, and the percentage of dead cells was then determined by the number of nuclei presenting high levels of TO-PRO-3 staining. Intracellular esterase activity was evaluated by Calcein-AM staining.⁵

The following filter blocks were configured for excitation and emission during the fluorescence microscopy analysis:

- Calcein-AM: The filter block was set for excitation at wavelengths of 460–490 nm and for emission at wavelengths of 500–550 nm.
- DAPI: The filter block was adjusted for excitation at wavelengths of 360–400 nm and for emission at wavelengths of 410–480 nm.
- TO-PRO-3: The filter block was configured for excitation at wavelengths of 520–550 nm and for emission at wavelengths of 650–760 nm.

Cytotoxicity assays. In short, the HFF-1 cells were plated at a density of 1x10⁴ cells/well in a 96-well plate at 37 °C in 5 % CO₂ atmosphere (200 µl per well, number of repetitions = 5). After 24

h of culture, the medium in the wells was replaced with fresh medium containing magnetic nanoparticles in varying concentrations from 0.1 $\mu\text{g/ml}$ to 100 $\mu\text{g}_{\text{Fe}}/\text{ml}$. After 24 h, the supernatant of each well was replaced by 200 μl of fresh medium with 3-[4,5-dimethylthiazol-2-yl]-2,5-diphenyl tetrazolium bromide (MTT) (0.5 mg/mL). After 2 h of incubation at 37 °C and 5 % CO_2 , the medium was removed, the formazan crystals were solubilized with 200 μl of DMSO, and the solution was vigorously mixed to dissolve the reacted dye. The absorbance of each well $[\text{Abs}]_{\text{well}}$ was read on a microplate reader (Dynatech MR7000 instruments) at 550 nm. The relative cell viability (%) and its error related to control wells containing cell culture medium without nanoparticles were calculated by the equations:

$$RCV(\%) = \left(\frac{[\text{Abs}]_{\text{test}} - [\text{Abs}]_{\text{Pos.Ctrl.}}}{[\text{Abs}]_{\text{Neg.Ctrl.}} - [\text{Abs}]_{\text{Pos.Ctrl.}}} \right) \times 100$$

$$Error(\%) = RCV_{\text{test}} \times \sqrt{\left(\frac{\sigma_{\text{test}}}{[\text{Abs}]_{\text{test}}} \right)^2 + \left(\frac{\sigma_{\text{Ctrl}}}{[\text{Abs}]_{\text{Ctrl.}}} \right)^2}$$

where σ is the standard deviation. Triton X-100 was added to the positive control wells.

f) Animal Housing and Care

Mice were housed in individually ventilated cages (IVCs) under controlled environmental conditions: temperature of $21 \pm 2^\circ\text{C}$, relative humidity of $55 \pm 10\%$ and a 12-hour light/dark cycle (lights on at 08:00). Up to 5 animals were housed per cage, depending on the experimental protocol and social compatibility.

Animals had ad libitum access to standard laboratory chow and filtered tap water. Bedding was changed twice weekly, and environmental enrichment (e.g., nesting material, cardboard shelters) was provided throughout the experiment to promote well-being and natural behavior. All animals were acclimatized for at least 7 days prior to experimentation. Health status was monitored daily by trained personnel, and humane endpoints were applied in accordance with ethical standards.

g) *In vivo* Magnetic Resonance Imaging (MRI).

Mice were anesthetized with 1% isoflurane before being placed in the magnet, and the tail vein was cannulated. Respiration and body temperature were monitored throughout the entire experiment. NPs were administered intravenously at a concentration of 15 mg (Fe) per kg. All the MRI experiments were conducted on a 9.4 T Bruker Biospec system equipped with 400 mT/m gradients and a 40 mm quadrature bird-cage resonator. *In vivo* pharmacokinetics and biodistribution were studied as previously described by our group.⁶

The MRI acquisition scheme was as follows:

1. High-resolution T_2 -weighted images (0 h)

2. T₂ parametric images (0 h)
3. Intravenous injection of the nanoparticles
4. Dynamic T₂-weighted sequence
5. High-resolution T₂-weighted images (1 h)
6. T₂ parametric images (1 h)

High-resolution T₂-weighted images were acquired using a turbo-RARE sequence with respiratory gating (TE = 27 ms, TR = 1000 ms, 4 averages, 156 μm in-plane resolution, and 1 mm slice thickness).

Quantitative T₂ measurements were also performed using a multi-echo spin-echo CPMG sequence (TEs ranging from 7 ms to 448 ms, TR = 3500 ms, FOV = 4 cm, matrix size = 128x128, slice thickness = 1 mm).

Dynamic T₂-weighted MRI was performed using a turbo-RARE sequence with the same parameters indicated above, but only 1 average to improve temporal resolution (1 image every 30 seconds).

Dynamic T₂-weighted MRI was analyzed semiquantitatively using the following expression:

$$RE = \left| \frac{I_t - I_0}{I_0} \times 100 \right|$$

where RE is the modulus of relative signal enhancement, I_t is the signal intensity at any given time after the nanoparticle injection, and I_0 is the signal intensity before the injection.

Pharmacokinetics were obtained from the dynamic T₂-weighted sequences by calculating the average RE values within different regions of interest (ROIs) on the following tissues: liver, spleen, and kidneys.

Quantitative in vivo evaluation of NPs biodistribution was performed by calculating the average relaxation rate ($R_2=1/T_2$) within ROIs outlined on R₂ maps obtained from the CPMG sequences.

h) AC Susceptibility Measurements

Magnetic characterization was performed using dried solid samples placed directly into gelatin capsules. To obtain these solid samples, tissues and blood were freeze-dried until complete dehydration for at least 24 h. Magnetic susceptibility measurements were performed in a Quantum Design (USA) MPMS-XL SQUID magnetometer with an AC (alternating current) amplitude of 4.1 Oe at a frequency of 11 Hz. Full measurements were performed in the temperature range between 2 and 300 K to identify and quantify the presence of IONPs in the tissues. Shorter measurements in additional animals were performed in the 70–120 K temperature range, near the IONP maximum signal in out-of-phase magnetic susceptibility.

i) Blood Collection Process

At the end of the experiment, while the animal remained anesthetized, it was carefully placed in a holder. Then, a needle was gently inserted into the thoracic cavity at the point of maximum heartbeat strength. Once blood became visible in the hub of the needle, the syringe was stabilized, and blood was withdrawn slowly and steadily. A portion of the blood was dried for AC Susceptibility Measurements. The remaining blood was placed in a heparinized Eppendorf tube and centrifuged at 10.000 r.p.m. for 10 minutes, after which the supernatant (blood serum) was collected for subsequent TEM and TD-NMR analysis.

j) Histology

The tissues were fixed in 4% formaldehyde (Panreac, pH 7 buffered) for 48 h, changing the 4% formaldehyde after 24 h. Then, the samples were dehydrated through graded ethanol and embedded in paraffin (temperature 56 °C for 2 h under stirring and vacuum). Histological analysis was conducted using a LEICA APERIO VERSA 200 in light microscopy mode. The detailed procedures are described below.

Haematoxylin and Eosin (H&E): paraffin-embedded samples were sectioned at 7 µm thickness, then, from deparaffinization to mounting on commercial glass slides, the following protocol was conducted: Xylene (2 minutes), Xylene (2 minutes), 100% ethanol (2 minutes), 100% ethanol (2 minutes), 95% ethanol (2 minutes), water wash (2 minutes), Hematoxylin (3 minutes), water wash (1 minute), acid alcohol solution (1 minute), water wash (1 minute), bluing (1 minute), water wash (1 minute), 95% ethanol (1 minutes), Eosin (45 seconds), 95% ethanol (1 minutes), 100% ethanol (2 minutes), 100% ethanol (2 minutes), Xylene (2 minutes), Xylene (2 minutes). including detailed time points. Finally, tissue sections were mounted on commercial glass slides.

Prussian Blue (PB): paraffin-embedded samples were sectioned at 7 µm thickness, then deparaffinized, rehydrated, submerged in 20% hydrochloric acid and 10% potassium ferrocyanide, washed with water, and counterstained with Nuclear Fast Red, dehydrated in ascending concentrations of ethanol, cleared in xylene and mounted in commercial glass slide.

2. RESULTS

a) Characterization

Iron oleate

FTIR peaks (cm^{-1}): 2920 (CH_2 symmetric stretch vibration), 2840 (CH_3 stretch vibration), 1580 ($\text{C}=\text{C}$ stretch vibration), 1425 ($\text{C}-\text{O}$ stretch vibration and $\text{C}-\text{C}$ stretch vibration).

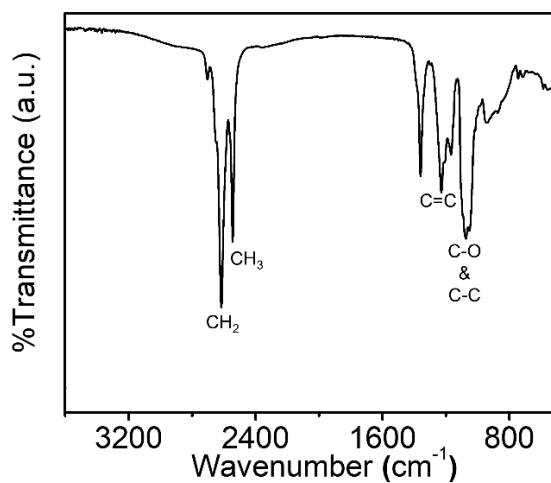


Figure S1. FTIR spectrum of iron oleate.

GA-PEG3000-OH ligand

^1H NMR (400 MHz, CDCl_3) δ (ppm): 7.22 (s, 2H), 4.43-4.40 (m, 2H), 3.85-3.45 (m, $\text{CH}_2\text{-PEG}$, -OH).

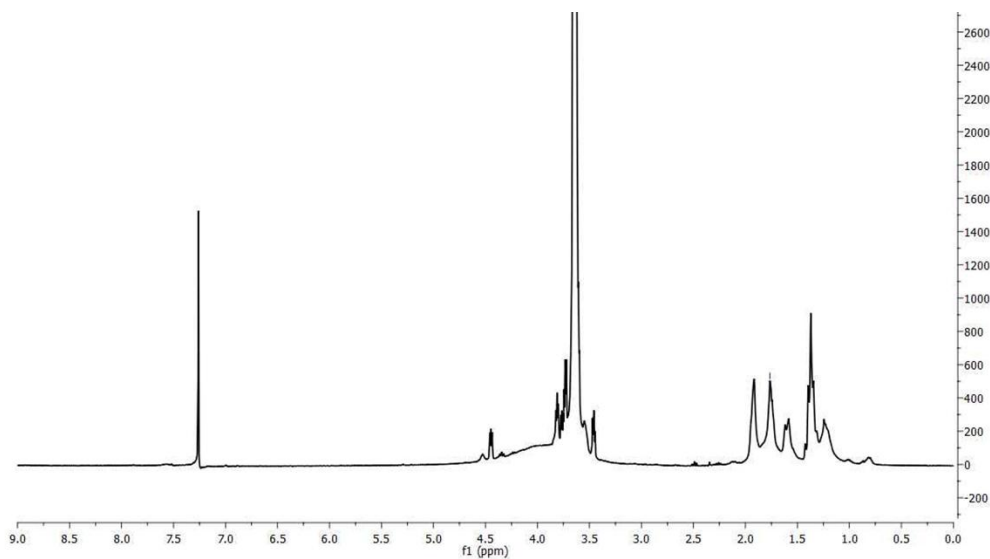


Figure S2. NMR spectrum of ligand GA-PEG3000-OH in CDCl_3 .

FTIR peaks (cm^{-1}): 1466 (C-H bend vibration), 1359 (C-H bend vibration), 1341 (C-H bend vibration), 1307 (anti-symmetric stretch vibration), 1268 (C-O stretch vibration), 1238 (C-O stretch vibration), 1092 (C-O-C stretch vibration), 942 (CH out-of-plane bending vibration).

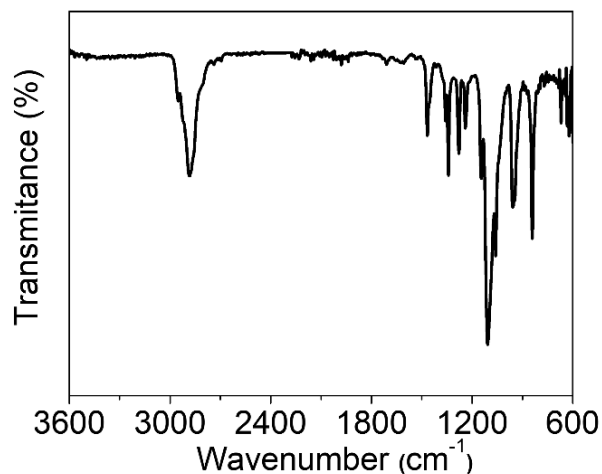


Figure S3. FTIR spectra of ligand GA-PEG3000-OH.

IONPs

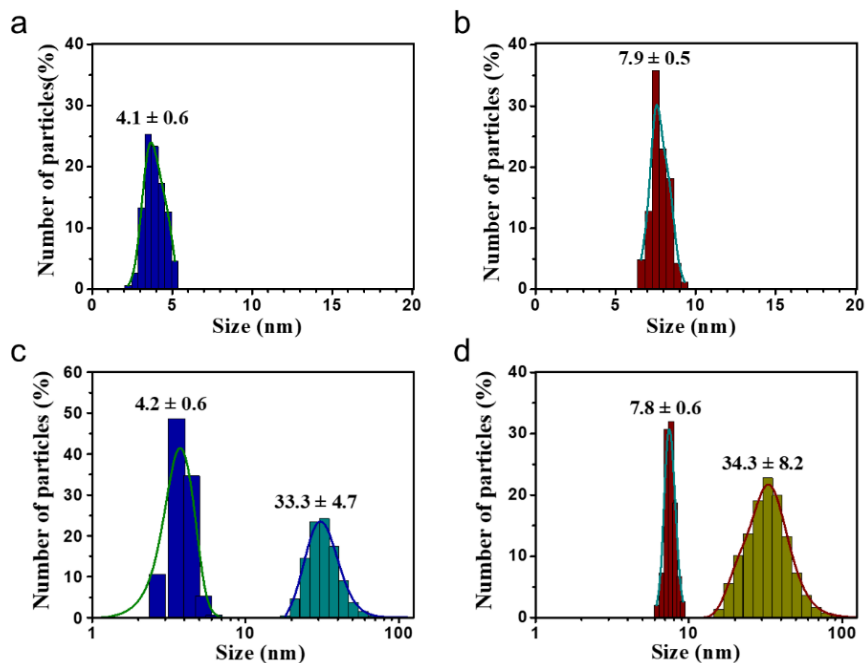


Figure S4. Representative histograms of sizes measured via TEM images of IONPs₁ (a) and IONPs₂ (b). Representative histograms of sizes measured via TEM images and HDs of functionalized IONPs₁ (c) and IONPs₂ (d). TEM sizes were calculated considering at least 100 particles.

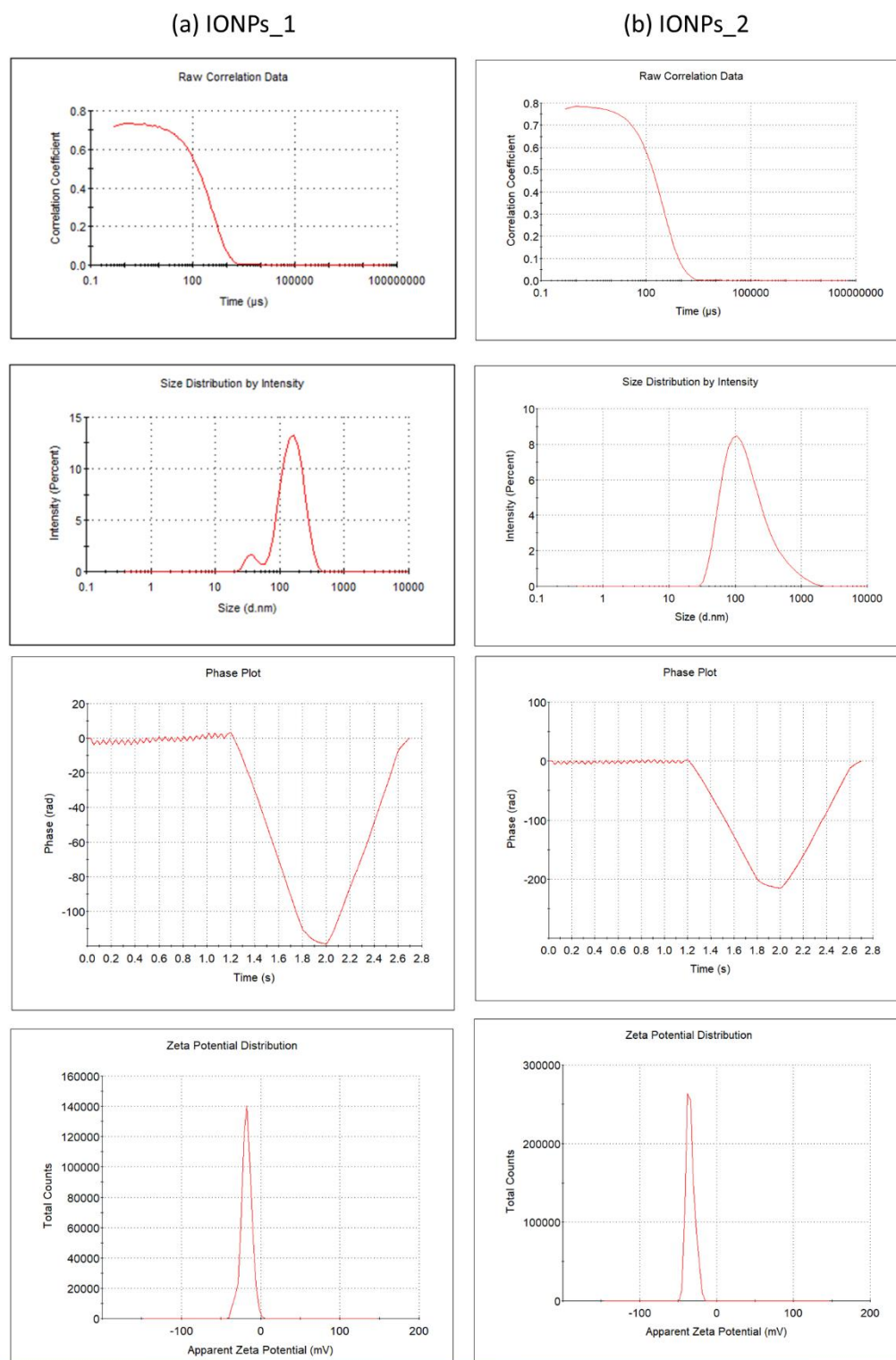


Figure S5. Average of correlation data, size distribution (by intensity), phase plot, and Zeta potential distribution for (a) IONPs_1 (4 nm) and (b) IONPs_2 (8 nm).

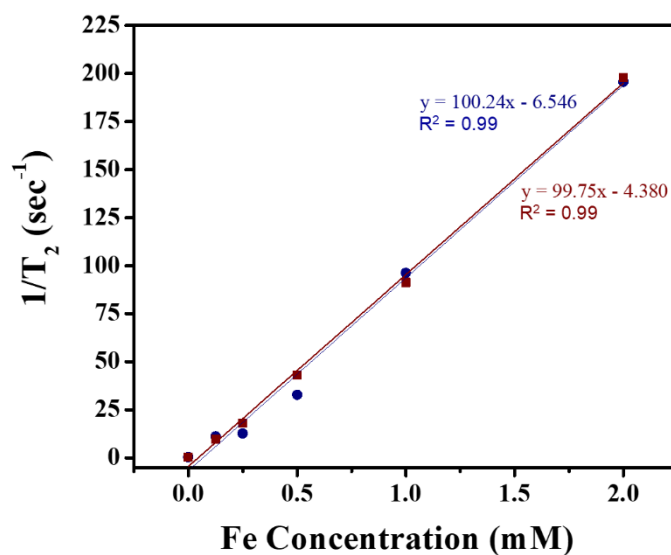


Figure S6. Plot of $1/T_2$ over Fe concentration for functionalized IONPs₁ (blue) and IONPs₂ (red) measured at 1.44 T. r_2 values correspond to the slope of the linear fit.

c) Protein corona analysis

Molecular function:
Binding subgroup

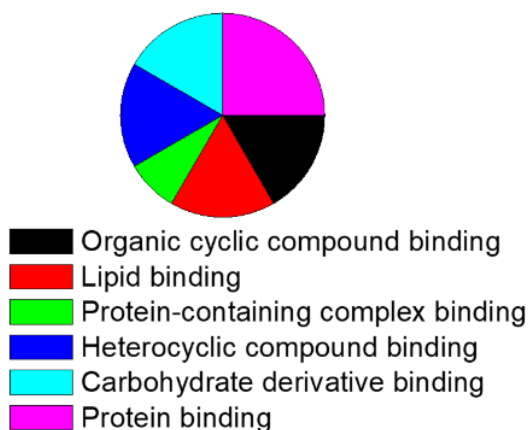


Figure S7. Pie charts representing the percentage of proteins based on ontology given by PANTHER for the unique proteins present around IONPs₁ with binding molecular function.

The list of the proteins unique to IONPs_1 is listed below:

Accession	Description
P07455	Insulin-like growth factor I
Q3MHY1	Cysteine and glycine-rich protein 1
P00744	Vitamin K-dependent protein Z
P79251	V-type proton ATPase subunit G 1
P54229	Cathelicidin-5
P10103	High mobility group protein B1
Q3T0D0	Heterogeneous nuclear ribonucleoprotein K
A2VE99	Septin-11
Q3T0M7	Ran-specific GTPase-activating protein
Q08E11	Peptidyl-prolyl cis-trans isomerase C
Q3T0V7	Endothelial differentiation-related factor 1
O18979	Neuroendocrine secretory protein 55
Q2HJH2	Ras-related protein Rab-1B
A1A4Q2	Prolyl-tRNA synthetase associated domain-containing protein 1
F1N152	Serine protease HTRA1
Q58CX7	Divergent protein kinase domain 2B
Q2YDE9	Testin

The list of all the common proteins is listed below:

Accession	Description
P56651	Inter-alpha-trypsin inhibitor heavy chain H2
P00829	ATP synthase subunit beta, mitochondrial
A2I7N0	Serpin A3-4
Q2KJ39	Reticulocalbin-3
Q29437	Primary amine oxidase, liver isozyme
Q3MHN5	Vitamin D-binding protein
Q3SZR3	Alpha-1-acid glycoprotein
Q2KIU3	Protein HP-25 homolog 2
P12763	Alpha-2-HS-glycoprotein
P19660	Cathelicidin-2
Q29443	Serotransferrin
Q9TTE1	Serpin A3-1
Q3T0F5	Ras-related protein Rab-7a
P02769	Albumin
A6QPQ2	Serpin A3-8

A2I7N3	Serpin A3-7
Q58CQ9	Pantetheinase
Q2KJF1	Alpha-1B-glycoprotein
P18902	Retinol-binding protein 4
P41361	Antithrombin-III
A2I7N2	Serpin A3-6
Q2KIT0	Protein HP-20 homolog
P49951	Clathrin heavy chain 1
O46406	Primary amine oxidase, lung isozyme
P02453	Collagen alpha-1(I) chain
P80012	von Willebrand factor
P81287	Annexin A5
Q3Y5Z3	Adiponectin
P01888	Beta-2-microglobulin
Q58D62	Fetuin-B
P28782	Protein S100-A8
P27674	Solute carrier family 2, facilitated glucose transporter member 1
P34955	Alpha-1-antiproteinase
G3MYZ3	Afamin
Q3SZV7	Hemopexin
P08169	Cation-independent mannose-6-phosphate receptor
Q3T004	Serum amyloid P-component
P58352	Solute carrier family 2, facilitated glucose transporter member 3
P30932	CD9 antigen
P00432	Catalase
P07224	Vitamin K-dependent protein S
Q3ZCL8	SH3 domain-binding glutamic acid-rich-like protein 3
P62261	14-3-3 protein epsilon
O46415	Ferritin light chain
A4FV54	Ras-related protein Rab-8A
Q3SZ57	Alpha-fetoprotein
Q3ZCJ8	Dipeptidyl peptidase 1
P31836	Neural cell adhesion molecule 1
P80109	Phosphatidylinositol-glycan-specific phospholipase D
P02465	Collagen alpha-2(I) chain
Q7SIH1	Alpha-2-macroglobulin
P42916	Collectin-43
P53712	Integrin beta-1
Q27991	Myosin-10
P54228	Cathelicidin-6
P00978	Protein AMBP

A7E3W2	Galectin-3-binding protein
P68252	14-3-3 protein gamma
Q08DP0	Phosphoglucomutase-1
P28800	Alpha-2-antiplasmin
P80189	Lysozyme C, non-stomach isozyme
P22457	Coagulation factor VII
P62871	Guanine nucleotide-binding protein G(I)/G(S)/G(T) subunit beta-1
P22226	Cathelicidin-1
P07589	Fibronectin
O46375	Transthyretin
Q5I597	Betaine--homocysteine S-methyltransferase 1
Q32LP0	Fermitin family homolog 3
Q3T052	Inter-alpha-trypsin inhibitor heavy chain H4
P48644	Aldehyde dehydrogenase 1A1
Q07130	UTP--glucose-1-phosphate uridylyltransferase
P04985	Elastin
Q29451	Lysosomal alpha-mannosidase
P56652	Inter-alpha-trypsin inhibitor heavy chain H3
Q3SZF2	ADP-ribosylation factor 4
Q08DA1	Sodium/potassium-transporting ATPase subunit alpha-1
Q0VCM5	Inter-alpha-trypsin inhibitor heavy chain H1
Q9TT36	Thyroxine-binding globulin
Q6URK6	Cadherin-5
Q2HJ86	Tubulin alpha-1D chain
Q2KIG3	Carboxypeptidase B2
P00743	Coagulation factor X
Q17QH6	Collectin-11
Q29RU4	Complement component C6
Q2UVX4	Complement C3
Q8SPP7	Peptidoglycan recognition protein 1
Q3MHN2	Complement component C9
Q0VCK0	Bifunctional purine biosynthesis protein ATIC
Q3MHP2	Ras-related protein Rab-11B
P35445	Cartilage oligomeric matrix protein
P0CH28	Polyubiquitin-C
Q3ZCJ2	Aldo-keto reductase family 1 member A1
Q58CS8	N-acetylglucosamine-1-phosphotransferase subunit gamma
Q28106	Contactin-1
Q27975	Heat shock 70 kDa protein 1A
Q9BGI3	Peroxiredoxin-2
Q32KY0	Apolipoprotein D

P13605	Fibromodulin
Q95JC7	Neutral amino acid transporter B(0)
P06868	Plasminogen
Q1JP75	L-xylulose reductase
Q5EA20	4-hydroxyphenylpyruvate dioxygenase
P63103	14-3-3 protein zeta/delta
A5D7I4	Exostosin-1
Q2KJD0	Tubulin beta-5 chain
E1BF81	Corticosteroid-binding globulin
Q05716	Insulin-like growth factor-binding protein 4
A6H768	Galactokinase
Q28065	C4b-binding protein alpha chain
Q5E9I6	ADP-ribosylation factor 3
P00735	Prothrombin
Q76LV1	Heat shock protein HSP 90-beta
P01030	Complement C4
P17690	Beta-2-glycoprotein 1
P61223	Ras-related protein Rap-1b
Q5E9H0	Phospholipase A1 member A
O77783	Exostosin-2
Q2HJ57	Coactosin-like protein
O77742	Osteomodulin
Q32PI5	Serine/threonine-protein phosphatase 2A 65 kDa regulatory subunit A alpha isoform
P17697	Clusterin
A7YY28	Putative protein-lysine deacylase ABHD14B
P19120	Heat shock cognate 71 kDa protein
Q0VCX1	Complement C1s subcomponent
Q2T9S0	Tubulin beta-3 chain
Q2KJ83	Carboxypeptidase N catalytic chain
Q5EA79	Galactose mutarotase
Q3SX14	Gelsolin
P01017	Angiotensinogen
P02584	Profilin-1
Q76LV2	Heat shock protein HSP 90-alpha
Q9N2I2	Plasma serine protease inhibitor
P23805	Conglutinin
P60712	Actin, cytoplasmic 1
Q9XSG3	Isocitrate dehydrogenase [NADP] cytoplasmic
Q3MHM5	Tubulin beta-4B chain
P60661	Myosin light polypeptide 6

Q5EA01	Beta-1,4-glucuronyltransferase 1
Q2HJF4	Phenazine biosynthesis-like domain-containing protein
P81948	Tubulin alpha-4A chain
Q3SWW8	Thrombospondin-4
Q2HJ49	Moesin
P01267	Thyroglobulin
Q3ZC09	Beta-enolase
Q05443	Lumican
Q5E9C0	Ras suppressor protein 1
Q0VCM4	Glycogen phosphorylase, liver form
Q3SZI4	14-3-3 protein theta
Q2KJC6	S-adenosylmethionine synthase isoform type-1
P50397	Rab GDP dissociation inhibitor beta
P33046	Cathelicidin-4
Q95M17	Acidic mammalian chitinase
P38657	Protein disulfide-isomerase A3
Q3T0P6	Phosphoglycerate kinase 1
P12260	Coagulation factor XIII A chain
Q92176	Coronin-1A
P40673	High mobility group protein B2
P19035	Apolipoprotein C-III
P16116	Aldo-keto reductase family 1 member B1
Q0VCU1	Cytoplasmic aconitate hydratase
Q95121	Pigment epithelium-derived factor
Q29RQ1	Complement component C7
P68250	14-3-3 protein beta/alpha
Q5E9E3	Complement C1q subcomponent subunit A
Q95122	Monocyte differentiation antigen CD14
Q5E947	Peroxiredoxin-1
Q3T145	Malate dehydrogenase, cytoplasmic
P81644	Apolipoprotein A-II
P00741	Coagulation factor IX
P80425	Fatty acid-binding protein, liver
Q2KJH9	4-trimethylaminobutyraldehyde dehydrogenase
Q56JW4	Adenine phosphoribosyltransferase
Q3SYV4	Adenylyl cyclase-associated protein 1
Q2KIV9	Complement C1q subcomponent subunit B
F1N2K1	Prenylcysteine oxidase 1
Q3T014	Bisphosphoglycerate mutase
P68138	Actin, alpha skeletal muscle
A3KMV5	Ubiquitin-like modifier-activating enzyme 1

P33072	Protein-lysine 6-oxidase
P54149	Mitochondrial peptide methionine sulfoxide reductase
O77834	Peroxiredoxin-6
P55052	Fatty acid-binding protein 5
Q5E9A1	Nascent polypeptide-associated complex subunit alpha
Q3ZBD7	Glucose-6-phosphate isomerase
P14568	Argininosuccinate synthase
P55906	Transforming growth factor-beta-induced protein ig-h3
P08037	Beta-1,4-galactosyltransferase 1
Q0VD19	Sphingomyelin phosphodiesterase
P31976	Ezrin
P52556	Flavin reductase (NADPH)
P21856	Rab GDP dissociation inhibitor alpha
P62998	Ras-related C3 botulinum toxin substrate 1
Q5EAD2	D-3-phosphoglycerate dehydrogenase
Q3T0S5	Fructose-bisphosphate aldolase B
P81187	Complement factor B
O02659	Mannose-binding protein C
P02672	Fibrinogen alpha chain
P28801	Glutathione S-transferase P
Q9XSJ4	Alpha-enolase
P52898	Dihydrodiol dehydrogenase 3
A7YWG4	Gamma-glutamyl hydrolase
Q3MHL4	Adenosylhomocysteinase
Q148F1	Cofilin-2
P02070	Hemoglobin subunit beta
Q3B7M9	Glycogen phosphorylase, brain form
P42899	60S acidic ribosomal protein P2
P02676	Fibrinogen beta chain
P61585	Transforming protein RhoA
Q3SYU2	Elongation factor 2
Q3T054	GTP-binding nuclear protein Ran
P28783	Protein S100-A9
P19534	Cadherin-2
Q3SZK8	Na(+)/H(+) exchange regulatory cofactor NHE-RF1
P10096	Glyceraldehyde-3-phosphate dehydrogenase
Q3ZC42	Alcohol dehydrogenase class-3
Q95M18	Endoplasmic reticulum chaperone protein BiP
P81134	Renin receptor
P50227	Sulfotransferase 1A1
P62803	Histone H4

Q2KJH4	WD repeat-containing protein 1
Q3SYW2	Complement C2
Q3SZE2	Prefoldin subunit 1
Q28178	Thrombospondin-1
P80311	Peptidyl-prolyl cis-trans isomerase B
P82943	Regakine-1
Q3SZJ4	Prostaglandin reductase 1
Q3SWY2	Integrin-linked protein kinase
Q5E9Z2	Hyaluronan-binding protein 2
Q5NTB3	Coagulation factor XI
A4IFA6	Immunoglobulin superfamily containing leucine-rich repeat protein
Q08E20	S-formylglutathione hydrolase
Q2KJ93	Cell division control protein 42 homolog
A4FUA8	F-actin-capping protein subunit alpha-1
P13753	BOLA class I histocompatibility antigen, alpha chain BL3-7
Q28085	Complement factor H
Q2M2T1	Histone H2B type 1-K
Q3ZBF7	Prostaglandin E synthase 3
P68103	Elongation factor 1-alpha 1
P00745	Vitamin K-dependent protein C
P19217	Sulfotransferase 1E1
Q29RU2	Oncoprotein-induced transcript 3 protein
P19034	Apolipoprotein C-II
Q0VCX2	Endoplasmic reticulum chaperone BiP
Q9XSC6	Creatine kinase M-type
Q6R8F2	Cadherin-1
O18738	Dystroglycan 1
Q2HJ60	Heterogeneous nuclear ribonucleoproteins A2/B1
Q9TTJ5	Regucalcin
P37141	Glutathione peroxidase 3
Q28035	Glutathione S-transferase A1
P19879	Mimecan
Q3SZX4	Carbonic anhydrase 3
P12378	UDP-glucose 6-dehydrogenase
Q3SZJ0	Argininosuccinate lyase
Q03247	Apolipoprotein E
P12799	Fibrinogen gamma-B chain
A7MBJ4	Receptor-type tyrosine-protein phosphatase F
Q3SZB7	Fructose-1,6-bisphosphatase 1
P11116	Galectin-1
Q9TU25	Ras-related C3 botulinum toxin substrate 2

Q2TA49	Vasodilator-stimulated phosphoprotein
Q32PJ2	Apolipoprotein A-IV
P01044	Kininogen-1
Q95M12	Legumain
A3KN12	Adenylosuccinate lyase
Q3SZV3	Elongation factor 1-gamma
Q3ZC84	Cytosolic non-specific dipeptidase
Q27967	Secreted phosphoprotein 24
Q2TBQ3	Guanidinoacetate N-methyltransferase
P46168	Beta-defensin 10
P04815	Spleen trypsin inhibitor I
Q27970	Calpain-1 catalytic subunit
Q5E946	Parkinson disease protein 7 homolog
Q3SZ62	Phosphoglycerate mutase 1
P07507	Matrix Gla protein
O18879	Glutathione S-transferase A2
Q5E9B7	Chloride intracellular channel protein 1
Q3T149	Heat shock protein beta-1
P05689	Cathepsin Z
Q28107	Coagulation factor V
P24627	Lactotransferrin
Q3SZD7	Carbonyl reductase [NADPH] 1
P50448	Factor XIIa inhibitor
Q2KIW9	UMP-CMP kinase
A5D989	Elongation factor 1-delta
P02081	Hemoglobin fetal subunit beta
P15497	Apolipoprotein A-I
P15467	Ribonuclease 4
P56425	Cathelicidin-7
P10575	Glutaredoxin-1
Q2NKY7	Septin-2
P01035	Cystatin-C
Q5E9E1	PDZ and LIM domain protein 1
Q0VCP3	Olfactomedin-like protein 3
Q9XTA3	Myocilin
P01045	Kininogen-2
Q2KIS7	Tetranectin
Q3ZBN5	Asporin
P98140	Coagulation factor XII
P05059	Chromogranin-A
P46170	Beta-defensin 12

Q5E9B1 L-lactate dehydrogenase B chain
 P19858 L-lactate dehydrogenase A chain
 P62958 Adenosine 5'-monophosphoramidase HINT1
 P17248 Tryptophan--tRNA ligase, cytoplasmic
 P13135 Calpain small subunit 1
 P98133 Fibrillin-1
 P62935 Peptidyl-prolyl cis-trans isomerase A
 Q06805 Tyrosine-protein kinase receptor Tie-1
 Q5E9A3 Poly(rC)-binding protein 1
 A2VE23 Dermokine
 Q5EA88 Glycerol-3-phosphate dehydrogenase [NAD(+)], cytoplasmic
 A6QQF6 Suprabasin
 Q9TS87 Transgelin
 Q27971 Calpain-2 catalytic subunit
 P09487 Alkaline phosphatase, tissue-nonspecific isozyme
 Q6B855 Transketolase
 Q24K22 Hepatocyte growth factor-like protein
 P13384 Insulin-like growth factor-binding protein 2
 P12624 Myristoylated alanine-rich C-kinase substrate
 Q3SZJ9 Phosphomannomutase 2
 Q5E984 Translationally-controlled tumor protein
 O18739 CCN family member 2
 Q2TBI0 Lipopolysaccharide-binding protein
 Q5E9F7 Cofilin-1
 P01966 Hemoglobin subunit alpha
 Q3ZBD9 Microtubule-associated protein RP/EB family member 1
 P48427 Tubulin-specific chaperone A
 A1A4R1 Histone H2A type 2-C
 Q2TBW7 Sorting nexin-2
 Q5E956 Triosephosphate isomerase
 P07456 Insulin-like growth factor II
 Q3SZ19 26S proteasome non-ATPase regulatory subunit 9
 A7MAZ5 Histone H1.3
 P80724 Brain acid soluble protein 1
 Q0P569 Nucleobindin-1
 Q2HJH9 Programmed cell death protein 5
 P13696 Phosphatidylethanolamine-binding protein 1
 Q05718 Insulin-like growth factor-binding protein 6
 Q28007 Dihydropyrimidine dehydrogenase [NADP(+)]
 P80221 C-X-C motif chemokine 6
 O62644 Leukocyte cell-derived chemotaxin-2

A6H767	Nucleosome assembly protein 1-like 1
Q5E9F5	Transgelin-2
Q58D31	Sorbitol dehydrogenase
P15246	Protein-L-isoaspartate(D-aspartate) O-methyltransferase
Q32P66	CXXC motif containing zinc binding protein
Q3T0A3	Complement factor D
P33433	Histidine-rich glycoprotein
Q3B7M5	LIM and SH3 domain protein 1
Q148C9	Heme-binding protein 1
P26884	Peptidyl-prolyl cis-trans isomerase FKBP3
Q5E9E2	Myosin regulatory light polypeptide 9
Q5E9D5	Dextrin
P24591	Insulin-like growth factor-binding protein 1
P35541	Serum amyloid A protein
P49907	Selenoprotein P
Q95LI2	Vitrin
Q6Q137	Septin-7
Q2KJ51	Angiopoietin-related protein 4
Q27976	Non-muscle caldesmon
Q3ZBZ8	Stress-induced-phosphoprotein 1
Q2KJ63	Plasma kallikrein
P10152	Angiogenin-1
P67808	Y-box-binding protein 1
P20959	Insulin-like growth factor-binding protein 3
P25975	Procathepsin L
Q3SYR5	Apolipoprotein C-IV
A5PKI3	Protein FAM3C
Q0VCU8	Eukaryotic translation initiation factor 3 subunit J
P79121	Metalloproteinase inhibitor 3
Q3SYU6	Calponin-2
Q2KJH6	Serpin H1
Q8MJ50	Osteoclast-stimulating factor 1
Q2KHW7	Regulator of G-protein signaling 10
A6H7G2	Drebrin-like protein
Q05717	Insulin-like growth factor-binding protein 5
Q32L76	Serum amyloid A-4 protein
Q5E983	Elongation factor 1-beta
Q9GLX9	Spondin-1
Q3ZBV8	Threonine--tRNA ligase 1, cytoplasmic
Q0VFX8	Cysteine-rich protein 2

PepStat analysis:**Table S2.** Protein residues uniquely adsorbed on IONP_1 and commonly adsorbed on both IONPs, analyzed using PepStat, and expressed as mole percentages.

Residue	Unique (mole%)	Common (mole%)
A = Ala	6.8	8.3
B = Asx	0.0	0.0
C = Cys	3.9	4.3
D = Asp	4.1	4.1
E = Glu	12.2	9.4
F = Phe	1.2	1.4
G = Gly	2.1	2.2
H = His	2.5	3.4
I = Ile	9.9	9.3
K = Lys	0.8	0.9
L = Leu	3.3	4.7
M = Met	1.4	2.7
N = Asn	9.9	9.2
P = Pro	5.4	6.2
Q = Gln	1.9	2.5
R = Arg	7.6	5.6
S = Ser	4.5	5.1
T = Thr	9.7	7.3
V = Val	1.2	0.5
W = Trp	0.2	0.2
Y = Tyr	2.3	2.1
Z = Glx	0.0	0.0

Table S3. The amino acid composition of proteins uniquely adsorbed on IONP_1 and commonly adsorbed on both IONPs was analyzed using PepStat and expressed as mole percentages.

Property	Residues	Unique (mole%)	Common (mole%)
Tiny	(A+C+G+S+T)	28.7	29.4
Small	(A+B+C+D+G+N+P+S+T+V)	49.3	49.4
Aliphatic	(A+I+L+V)	21.4	23.1
Aromatic	(F+H+W+Y)	6.2	7.1
Non-polar	(A+C+F+G+I+L+M+P+V+W+Y)	39.6	44.5
Polar	(D+E+H+K+N+Q+R+S+T+Z)	60.2	54.9
Charged	(B+D+E+H+K+R+Z)	34.2	30.8
Basic	(H+K+R)	17.9	17.4
Acidic	(B+D+E+Z)	16.3	13.5

c) Cell toxicity assessment

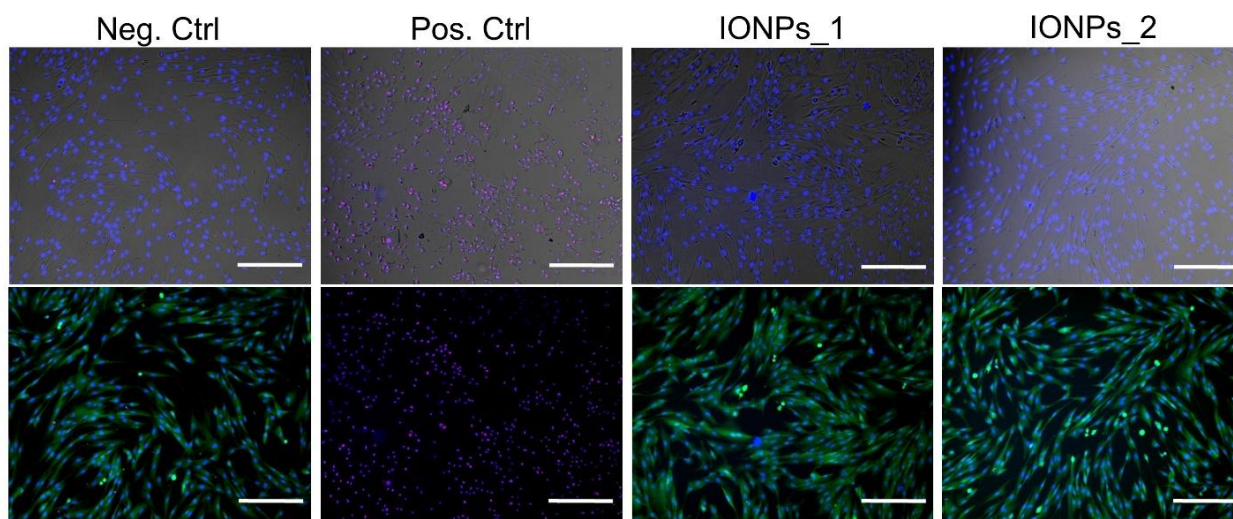


Figure S8. Representative optical microscopy images of HFF-1 without exposure (Neg. Ctrl), after exposure to 30% Ethanol (Pos. Ctrl), and after exposure to 100 $\mu\text{g}/\text{mL}$ (Fe concentration) of IONPs_1 and IONPs_2. The images show the merge of brightfield (grey) and DAPI (blue) and TO-PRO@-3 iodide (red) (TOP) and the merge of DAPI (blue), TO-PRO@-3 iodide (red), and Calcein AM (green). Scale bar =100 μm .

d) *In vivo* MRI studies

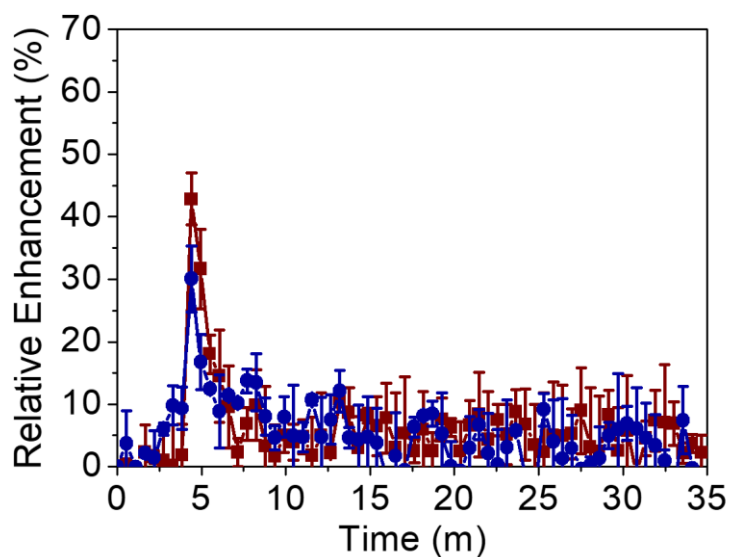


Figure S9. *In vivo* short-term time courses of relative enhancement in the kidneys of Balb/c mice following the intravenous administration of IONPs_1 (blue) or IONPs_2 (red), as determined by dynamic T2-weighted MRI.

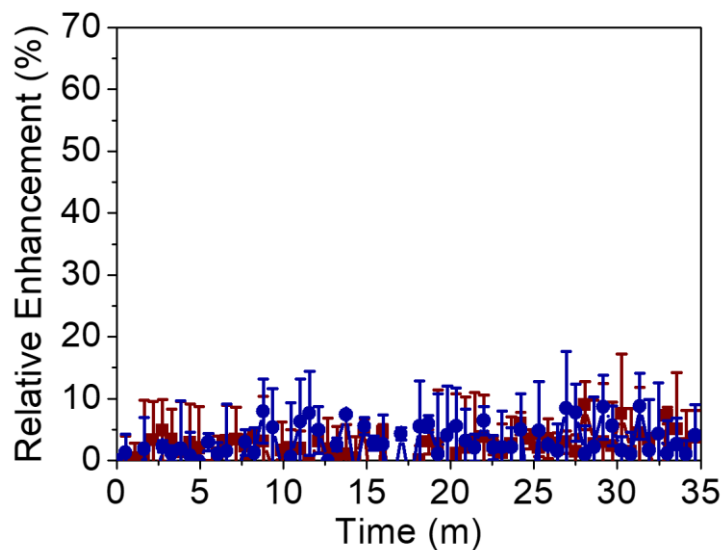


Figure S10. *In vivo* short-term time courses of relative enhancement in the muscle of Balb/c mice following the intravenous administration in mice of IONPs_1 (blue) or IONPs_2 (red), as determined by dynamic T2-weighted MRI.

e) AC susceptibility measurements

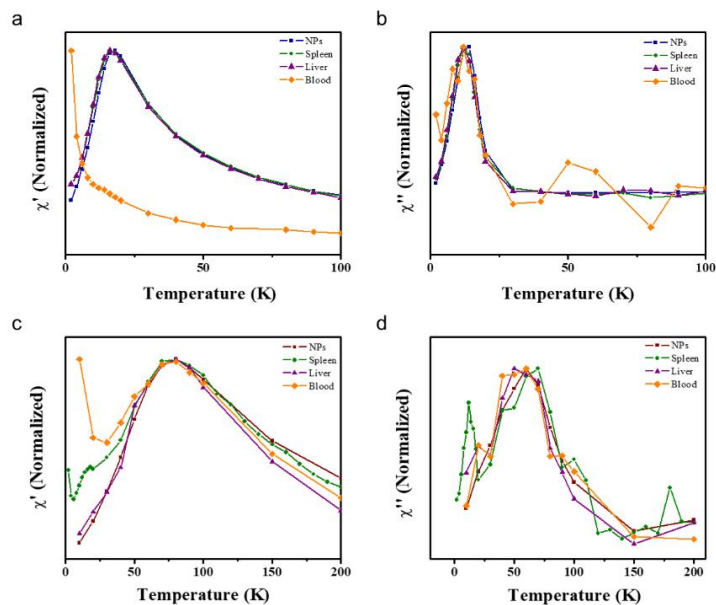


Figure S11. Curves for in-phase χ' (T) (a,c) and out of phase χ'' (T) (b,d) normalized magnetic susceptibility components for IONPs_1 (a,b) or IONPs_2 (c,d).

f) Histology

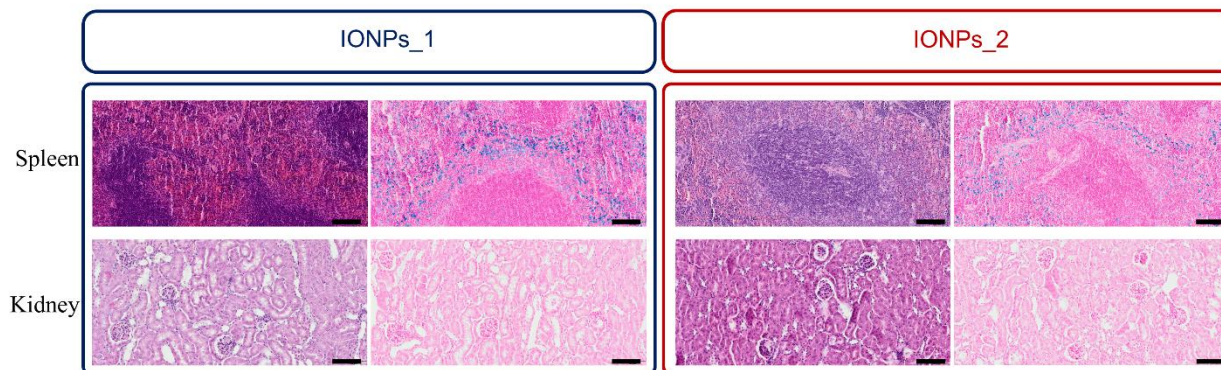


Figure S12. Representative histological sections of the spleen (top) and kidneys (bottom) of Balb/c mice intravenously injected with IONPs_1 (blue) and IONPs_2 (red). Images show the staining with H&E (left) and PB (right). The scale bar corresponds to 100 μm .

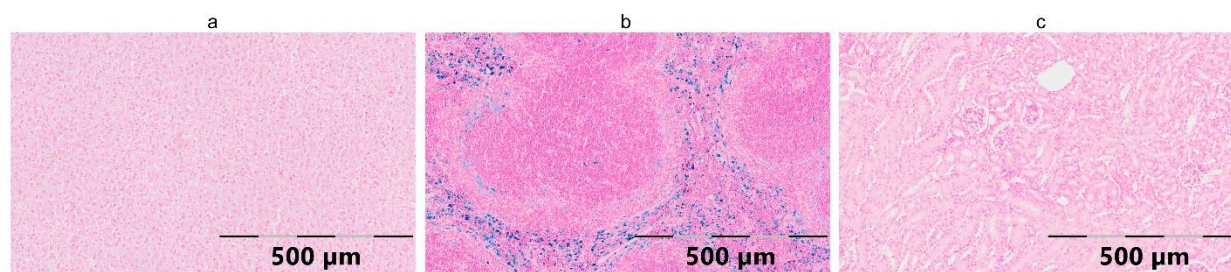


Figure S13. Representative histological sections of the liver (a), spleen (b) and kidney (c) of non-injected mice.

References

1. E. Pozo-Torres, C. Caro, A. Avasthi, J. M. Paez-Munoz, M. L. Garcia-Martin, I. Fernandez and M. Pernia Leal, *Soft Matter*, 2020, **16**, 3257-3266.
2. L. Shi, J. Zhang, M. Zhao, S. Tang, X. Cheng, W. Zhang, W. Li, X. Liu, H. Peng and Q. Wang, *Nanoscale*, 2021, **13**, 10748-10764.
3. V. B. Damodaran, C. J. Fee, T. Ruckh and K. C. Popat, *Langmuir*, 2010, **26**, 7299-7306.
4. L. M. Rodriguez-Perez, B. Ojeda-Pérez, J. López-de-San-Sebastián, M. García-Bonilla, M. González-García, B. Fernández-Muñoz, R. Sánchez-Pernaute, M. L. García-Martín, D. Domínguez-Pinos, C. Cárdenas-García, A. J. Jiménez and P. Paez-Gonzalez, *Stroke*, 2024, **55**, 1062-1074.
5. S. Neri, E. Mariani, A. Meneghetti, L. Cattini and A. Facchini, *Clinical Diagnostic Laboratory Immunology*, 2001, **8**, 1131-1135.
6. C. Caro, M. Carmen Munoz-Hernandez, M. P. Leal and M. L. Garcia-Martin, *Methods Mol Biol*, 2018, **1718**, 409-419.